

SUPPORTING INFORMATION

Selenolate-Protected Au₃₈ Nanoclusters: Isolation and Structural Characterization

Wataru Kurashige,[†] Seiji Yamazoe,[‡] Keita Kanehira,[†] Tatsuya Tsukuda,[‡] and Yuichi Negishi*[†]

[†] Department of Applied Chemistry, Faculty of Science, Tokyo University of Science, 1-3 Kagurazaka, Shinjuku-ku, Tokyo 162-8601, Japan.

[‡] Department of Chemistry, Faculty of Science, University of Tokyo, 7-3-1 Hongo, Bunkyo-ku, Tokyo 113-0033, Japan.

I. Experimental Procedures

A. Chemicals

All chemicals were purchased commercially and used as-received without further purification. Hydrogen tetrachloroaurate tetrahydrate (HAuCl₄·4H₂O) was obtained from Tanaka Kikinokoku. Selenium (Se), dodecylbromide (C₁₂H₂₅Br), bromooctane (C₈H₁₇Br), 1-dodecanethiol (C₁₂H₂₅SH), tetraoctylammonium bromide ((C₈H₁₇)₄NBr), sodium tetrahydroborate (NaBH₄), ethanol, toluene, dichloromethane (CH₂Cl₂), acetone, acetonitrile and glutathione were obtained from Wako Pure Chemical Industries. *Trans*-2-[3-(4-*tert*-butylphenyl)-2-methyl-2-propenylidene] malononitrile (DCTB) was purchased from Santa Cruz Biotechnology. Tetrabutylammonium perchlorate ((C₄H₉)₄NClO₄) and phenylethanethiol (PhC₂H₄SH) were purchased from Tokyo Chemical Industry. Didodecyldiselenide ((C₁₂H₂₅Se)₂) and dioctyldiselenide ((C₈H₁₇Se)₂) were synthesized in our laboratory.¹ Deionized water with a resistivity of >18.2 MΩ cm was used throughout.

B. Synthesis

Au₃₈(SeC₁₂H₂₅)₂₄ was synthesized via a ligand-exchange reaction following a procedure similar to that used to synthesize phenylselenolate-protected Au₂₅ clusters (Au₂₅(SePh)₁₈) reported by Zhu.² The precursor cluster, Au₃₈(SC₂H₄Ph)₂₄ (Figures S1-S3),³⁻⁵ was synthesized using the method reported by Jin.⁶ In the initial step, 10 mg of Au₃₈(SC₂H₄Ph)₂₄ was dissolved in 5 mL acetone, following which 100 μL of (C₁₂H₂₅Se)₂ was added. After stirring for 6 h at room temperature, a black-green precipitate appeared. The mixture was then centrifuged at 3500 rpm to remove the precipitated Au₃₈(SeC₁₂H₂₅)₂₄ which was subsequently washed five times with ethanol. The octaneselenolate-protected Au₃₈ clusters (Au₃₈(SeC₈H₁₇)₂₄) used in this work for comparison purposes were synthesized using the same experimental procedures, except that (C₈H₁₇Se)₂ was used instead of (C₁₂H₂₅Se)₂.

We also attempted to use the Brust method⁷ to synthesize Au₃₈(SeC₁₂H₂₅)₂₄. We found that this method was not effective for the synthesis of this particular compound, implying that a ligand-exchange reaction is the effective method for the synthesis of the Au₃₈(SeC₁₂H₂₅)₂₄. Similarly, it is expected that ligand-exchange reactions are necessary for the synthesis of larger clusters, such as Au₁₀₂(SeC₁₂H₂₅)₄₄ and Au₁₄₄(SeC₁₂H₂₅)₆₀, since those clusters were also not synthesized by the Brust method in our experiments.

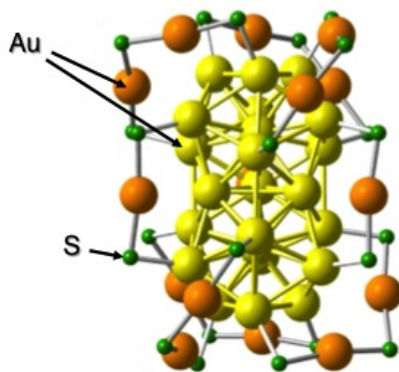


Figure S1. Structural representation of Au₃₈(SC₂H₄Ph)₂₄ determined by single-crystal X-ray analysis.³ The PhC₂H₄ moieties are omitted for clarity. Au₃₈(SR)₂₄ clusters synthesized with different ligands are believed to have similar geometrical structures.^{4,5}

C. Characterization

Electrospray ionization time-of-flight (ESI-TOF) mass spectra were recorded using a custom-designed mass spectrometer.⁸ A 1 mg/mL toluene/acetonitrile (7:3, v/v) solution of $\text{Au}_{38}(\text{SeC}_{12}\text{H}_{25})_{24}$ was electrosprayed at a flow rate of 120 $\mu\text{L}/\text{h}$. The charged liquid droplets were fed into a capillary and resistance heated to approximately 180 °C to form intact cluster ions via desolvation. The mass spectra were calibrated by reference to $\text{Na}_{n+1}\text{I}_n^+$ ions generated from NaI in methanol/water (1:1, v/v) solution. In the resulting mass spectra, $\text{Au}_{38}(\text{SeC}_{12}\text{H}_{25})_{24}$ was observed as a dication, $\text{Au}_{38}(\text{SeC}_{12}\text{H}_{25})_{24}^{2+}$. However, considering its similarity to $\text{Au}_{38}(\text{SC}_{12}\text{H}_{25})_{24}$, $\text{Au}_{38}(\text{SeC}_{12}\text{H}_{25})_{24}$ is expected to be present as the neutral species $[\text{Au}_{38}(\text{SeC}_{12}\text{H}_{25})_{24}]^0$ and we therefore also obtained an ESI mass spectrum while adding a small amount of $(\text{C}_8\text{H}_{17})_4\text{NBr}$ (Ref. 9) or $(\text{C}_4\text{H}_9)_4\text{NClO}_4$ (Ref. 10) to observe neutral species as the corresponding cations. Unfortunately the resulting ion intensity was very weak and an ion peak was not observed under these experimental conditions. Therefore, unlike in previous studies, we were unable to determine the charge state by this method.

Matrix-assisted laser desorption ionization (MALDI) mass spectra were acquired via a linear time-of-flight mass spectrometer (Applied Biosystems, Voyager Linear RD VDA 500) with a nitrogen laser (wavelength: 337 nm) using DCTB as the MALDI matrix.¹¹ The cluster-to-matrix ratio was set to 1:1000 and the laser fluence was reduced to the lowest value that enabled ions to be detected.

¹H nuclear magnetic resonance (NMR) analysis was conducted on a JEOL JNM-LA500 spectrometer using samples dissolved in CDCl_3 .

Thermogravimetric analysis (TGA; Bruker, TGA2000SA) was performed using 10.0 mg samples of $\text{Au}_{38}(\text{SeC}_{12}\text{H}_{25})_{24}$ or $\text{Au}_{38}(\text{SC}_{12}\text{H}_{25})_{24}$ at a heating rate of 10 °C/min under N_2 flow over the temperature range 25–500 °C.

Transmission electron microscopy (TEM) images were recorded using an electron microscope (Hitachi, H-7650) operating at 100 kV, typically with a magnification of 100,000.

Au L_3 -edges X-ray absorption fine structure (XAFS) measurements were carried out at the BL01B1 beam line at the SPring-8 facility of the Japan Synchrotron Radiation Research Institute (proposal no. 2012B1074). An Si(311) two-crystal monochromator was used for the incident beam. All spectra were recorded in the transmission mode and ion chambers were used as the I_0 and I detectors. $\text{Au}_{38}(\text{SeC}_{12}\text{H}_{25})_{24}$, $\text{Au}_{38}(\text{SC}_{12}\text{H}_{25})_{24}$, $\text{Au}_{25}(\text{SeC}_{12}\text{H}_{25})_{18}$ or $\text{Au}_{25}(\text{SC}_{12}\text{H}_{25})_{18}$ clusters diluted with KBr were placed between the ion chambers. Energy calibration was carried out using Cu foil for Au L_3 -edge analyses. Data analysis was performed with the REX2000 Ver. 2.5.9 software package (Rigaku Co.). The X-ray absorption near edge structure (XANES) data were analyzed by removing the atomic absorption background using a cubic spline from the χ spectra followed by normalization to the edge height. The extended X-ray absorption fine structure (EXAFS) data for the Au L_3 -edges were analyzed as follows. The χ spectra were extracted by removing the atomic absorption background using a cubic spline and were normalized to the edge height. The k^3 -weighted χ spectra underwent a Fourier transform (FT) into the r space using the FT range 3.0–13.5 \AA^{-1} . Curve fitting analysis was performed for the Au-Se (or S) and Au-Au bonds. The curve fitting range was 1.8–3.0 \AA for $\text{Au}_{38}(\text{SeC}_{12}\text{H}_{25})_{24}$ and $\text{Au}_{25}(\text{SeC}_{12}\text{H}_{25})_{18}$ and 1.5–3.0 \AA for $\text{Au}_{38}(\text{SC}_{12}\text{H}_{25})_{24}$ and $\text{Au}_{25}(\text{SC}_{12}\text{H}_{25})_{18}$. A passive electron factor (S_0^2) of 1 was used in this study. The phase and amplitude functions of Au-Se, Au-S and Au-Au bonds were extracted from AuSe {space group: P63/mmc, inorganic crystal structure database (ICSD)#52674}, Au₂S (space group: Pn3-m, ICSD#78718) and Au foil (space group: Fm-3m, ICSD#44362) using FEFF8.¹²

X-ray diffraction (XRD) measurements were performed on a diffractometer (Rigaku, Rint2500) using Cu-K α radiation ($\lambda=1.54 \text{\AA}$) with a reflection-free silicon plate (Rigaku) as a substrate.

UV-Vis absorption spectra of the clusters were acquired in toluene solutions at ambient temperature with a spectrometer (JASCO, V-630) and diffuse reflectance spectra of the cluster was acquired at ambient temperature with a separate spectrometer (JASCO, V-670). The wavelength-dependent optical data, $I(w)$, were converted to energy-dependent data, $I(E)$, using the following equation, which conserves the integrated spectral areas.

$$I(E) = I(w)/(\partial E/\partial w) \propto I(w) \times w^2$$

Cyclic voltammetry (CV) and differential pulse voltammetry (DPV) were performed at room temperature on 0.1 M solutions of clusters in $(\text{C}_4\text{H}_9)_4\text{NClO}_4$ (10 mg/3 mL) with an electrochemical analyzer (BAS, ALS610D). A glassy carbon working electrode and a Pt wire counter electrode were used and ferrocene was employed as an internal reference. The measurements were conducted under an Ar atmosphere.

D. Stability against decomposition in toluene solution

Throughout investigations of the resistance of the clusters against decomposition to assess their stability, an organic synthesizer (EYELA, PPS-2510) was used to precisely and reproducibly control the solution temperatures. During these trials, $\text{Au}_{38}(\text{SeC}_{12}\text{H}_{25})_{24}$ or $\text{Au}_{38}(\text{SC}_{12}\text{H}_{25})_{24}$ were dissolved in 10 mL toluene and the resulting solutions (1.0×10^{-5} M) were monitored on standing at high temperature (65–120 °C).

II. Results

Table S1. Au L₃-edge EXAFS fitting results for Au₂₅(SeC₁₂H₂₅)₁₈ and Au₂₅(SC₁₂H₂₅)₁₈.

sample	bond	CN	r (Å)	ΔDW	R factor (%)
Au ₂₅ (SeC ₁₂ H ₂₅) ₁₈	Au-Se	1.7(3)	2.433(2)	0.0002(6)	6.8
	Au-Au	0.9(7)	2.769(13)	0.0005(48)	
Au ₂₅ (SC ₁₂ H ₂₅) ₁₈	Au-S	1.7(2)	2.320(3)	0.0003(4)	2.8
	Au-Au	0.8(4)	2.760(8)	0.0003(21)	
Au foil	Au-Au	13.0(16)	2.848(3)	0.0012(5)	8.8

Numbers in parentheses are uncertainties (*e.g.*, 2.433(2) represents 2.433 ± 0.002).

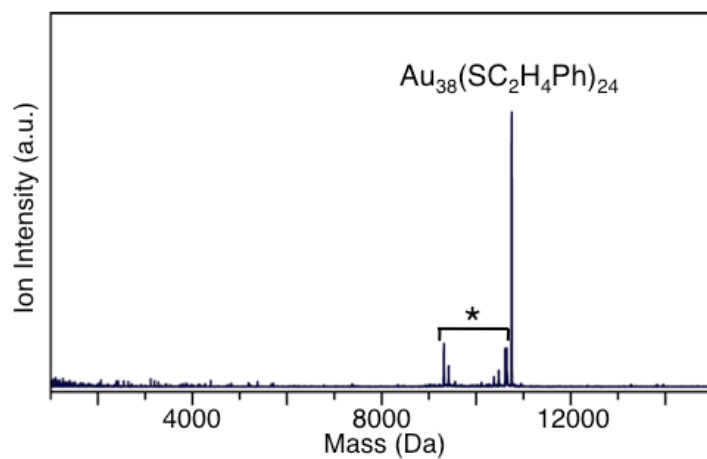


Figure S2. Positive-ion MALDI mass spectrum of the precursor cluster, $\text{Au}_{38}(\text{SC}_2\text{H}_4\text{Ph})_{24}$. The portion marked by an asterisk contains laser fragmentation ions.⁶

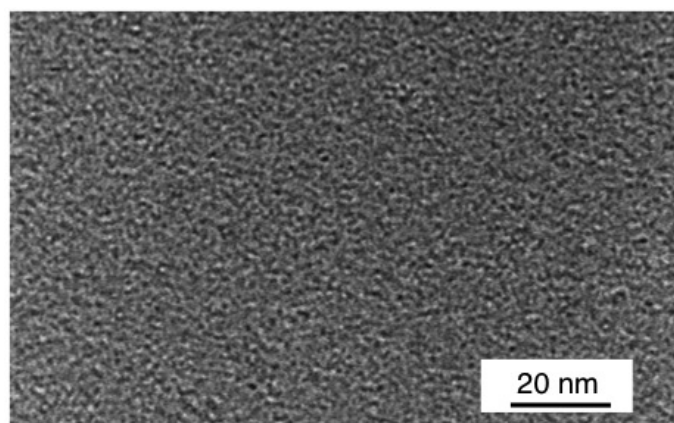


Figure S3. TEM image of $\text{Au}_{38}(\text{SC}_2\text{H}_4\text{Ph})_{24}$.

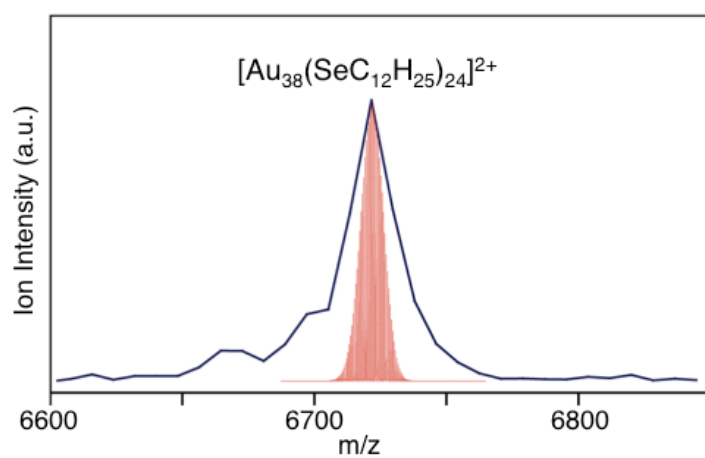


Figure S4. Enlarged positive-ion ESI mass spectrum of $\text{Au}_{38}(\text{SeC}_{12}\text{H}_{25})_{24}$ with the calculated isotope pattern for $[\text{Au}_{38}(\text{SeC}_{12}\text{H}_{25})_{24}]^{2+}$ (in red).

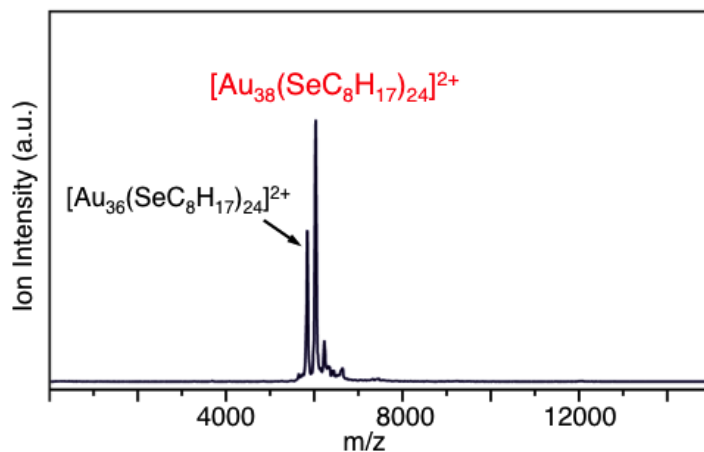


Figure S5. Positive-ion ESI mass spectrum of the products formed by the reaction between $\text{Au}_{38}(\text{SC}_2\text{H}_4\text{Ph})_{24}$ and $(\text{C}_8\text{H}_{17}\text{Se})_2$ (via ligand-exchange reaction). The main peak is assigned to $\text{Au}_{38}(\text{SeC}_8\text{H}_{17})_{24}$ ($[\text{Au}_{38}(\text{SeC}_8\text{H}_{17})_{24}]^{2+}$), supporting the assignment of the main peak observed in Figure 1(a).¹³ The peak assigned to $\text{Au}_{36}(\text{SeC}_8\text{H}_{17})_{24}$ ($[\text{Au}_{36}(\text{SeC}_8\text{H}_{17})_{24}]^{2+}$) was also observed in this mass spectrum. Since the relative ion intensities of $\text{Au}_{36}(\text{SeC}_8\text{H}_{17})_{24}$ and $\text{Au}_{38}(\text{SeC}_8\text{H}_{17})_{24}$ did not exhibit any variation with the experimental parameters of the mass spectrometer, this peak is not considered to be a fragment produced during the ionization process but rather a byproduct generated by the ligand-exchange reaction.¹⁴ An Au_{36} ($\text{Au}_{36}(\text{SeC}_{12}\text{H}_{25})_{24}$) cluster was not produced in the reaction between $\text{Au}_{38}(\text{SC}_2\text{H}_4\text{Ph})_{24}$ and $(\text{C}_{12}\text{H}_{25}\text{Se})_2$ (Figure 1(a)).

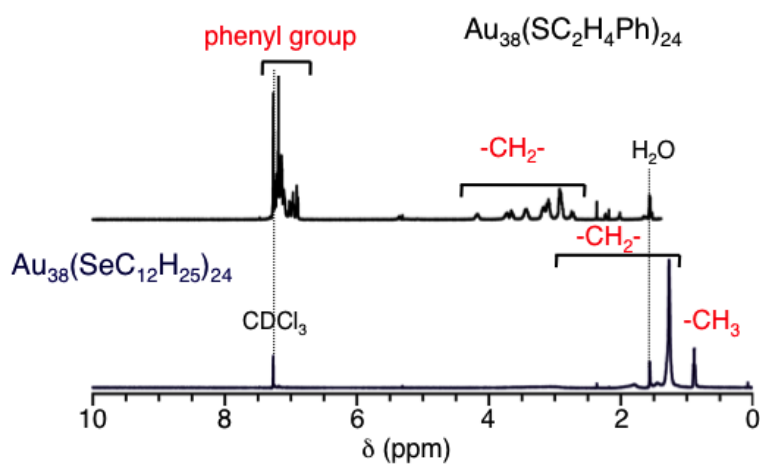


Figure S6. ^1H NMR spectra of $\text{Au}_{38}(\text{SC}_2\text{H}_4\text{Ph})_{24}$ and $\text{Au}_{38}(\text{SeC}_{12}\text{H}_{25})_{24}$. NMR assignments are based on literature data.^{15,16}

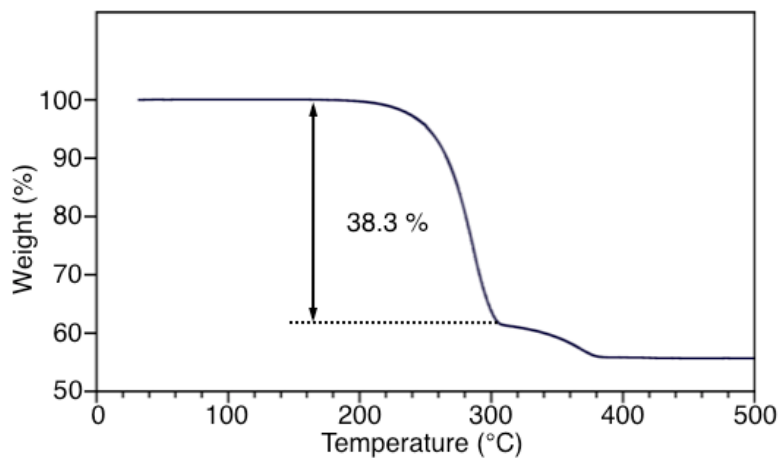


Figure S7. TGA data for Au₃₈(SeC₁₂H₂₅)₂₄. The shoulder is associated with a weight loss of 38.3 %. In the case of Au_{*n*}(SC₁₂H₂₅)_{*m*}, the alkyl chains begin to dissociate first.¹⁷ The shoulder observed here is not consistent with such dissociation, since in that case we would expect a weight loss of 30.2 %, corresponding to the weight ratio of alkyl chains in Au₃₈(SeC₁₂H₂₅)₂₄ of 30.2 %. A similar shoulder is also observed in the TGA curve of Au₂₅(SeC₁₂H₂₅)₁₈.¹⁸ A shoulder of this type is not seen, however, in the TGA plots obtained from Au₃₈(SC₁₂H₂₅)₂₄ (Figure S21) or Au₂₅(SC₁₂H₂₅)₁₈ (Ref. 18).

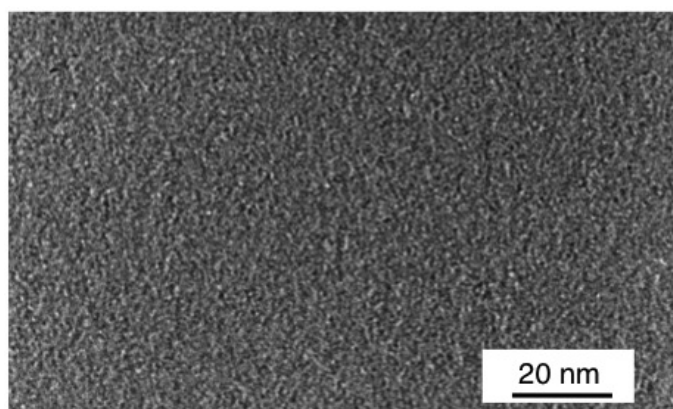


Figure S8. TEM image of Au₃₈(SeC₁₂H₂₅)₂₄.

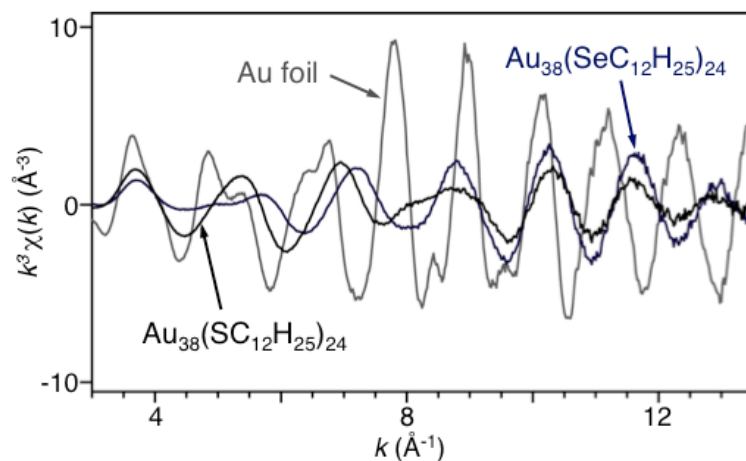


Figure S9. Au L_3 -edge EXAFS oscillations of $\text{Au}_{38}(\text{SeC}_{12}\text{H}_{25})_{24}$, $\text{Au}_{38}(\text{SC}_{12}\text{H}_{25})_{24}$ and Au foil.

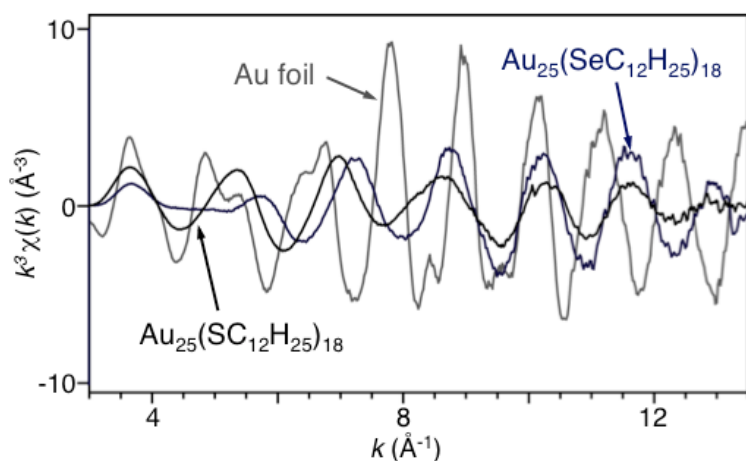


Figure S10. Au L_3 -edge EXAFS oscillations of $\text{Au}_{25}(\text{SeC}_{12}\text{H}_{25})_{18}$, $\text{Au}_{25}(\text{SC}_{12}\text{H}_{25})_{18}$ and Au foil.

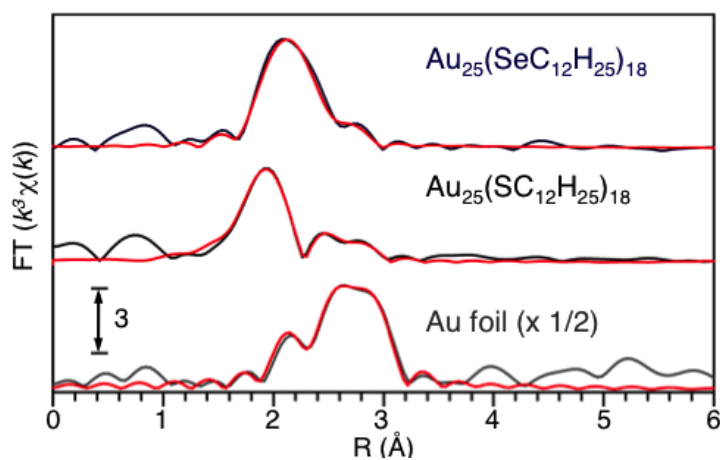


Figure S11. Experimental Au L_3 -edge FT-EXAFS data and best fits (red curves) for $\text{Au}_{25}(\text{SeC}_{12}\text{H}_{25})_{18}$, $\text{Au}_{25}(\text{SC}_{12}\text{H}_{25})_{18}$ and Au foil. Based on the EXAFS study of $\text{Au}_{25}(\text{SC}_2\text{H}_4\text{Ph})_{18}$ by Zhang,¹⁹ the peak around 2 Å is related to the Au-S bond and the peaks next to the Au-S bond in the higher R region are associated with Au-Au bonds in the FT-EXAFS data of $\text{Au}_{25}(\text{SC}_{12}\text{H}_{25})_{18}$.

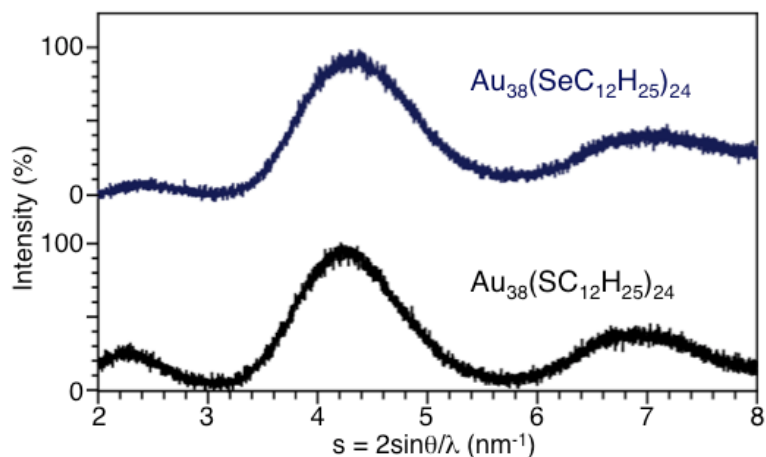


Figure S12. Powder XRD patterns of $\text{Au}_{38}(\text{SeC}_{12}\text{H}_{25})_{24}$ and $\text{Au}_{38}(\text{SC}_{12}\text{H}_{25})_{24}$.

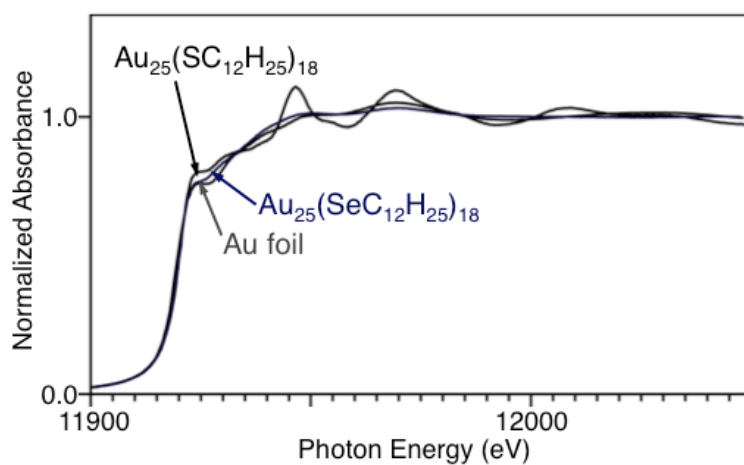


Figure S13. Au L_3 -edge XANES spectra of $\text{Au}_{25}(\text{SeC}_{12}\text{H}_{25})_{18}$, $\text{Au}_{25}(\text{SC}_{12}\text{H}_{25})_{18}$ and Au foil.

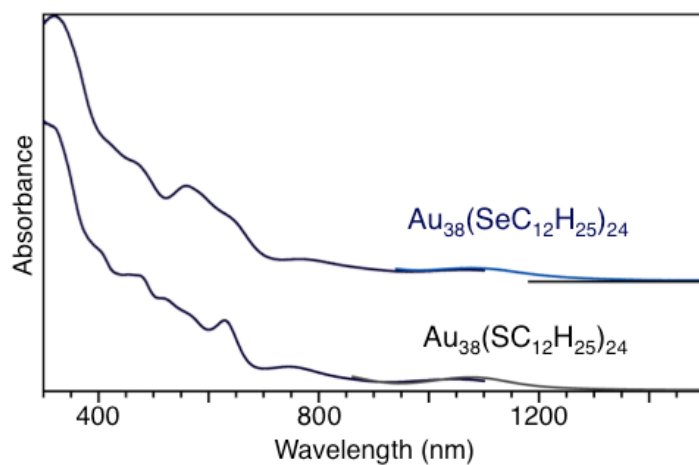


Figure S14. Optical absorption spectra of $\text{Au}_{38}(\text{SeC}_{12}\text{H}_{25})_{24}$ and $\text{Au}_{38}(\text{SC}_{12}\text{H}_{25})_{24}$. The superimposed spectra in the low energy region were obtained by diffuse reflectance spectroscopy of sample films.

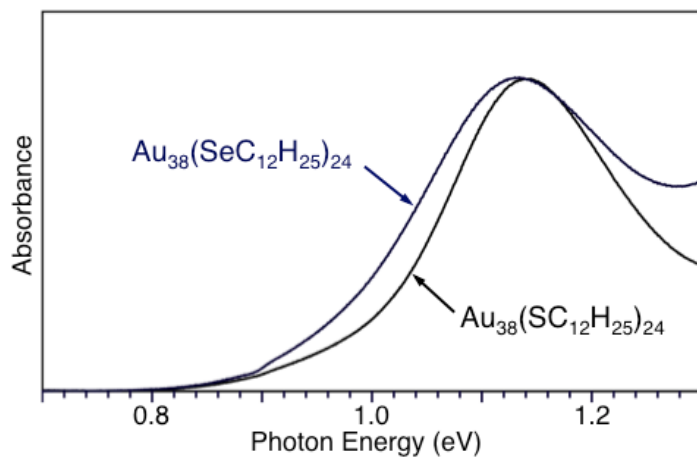


Figure S15. Enlarged optical absorption spectra of $\text{Au}_{38}(\text{SeC}_{12}\text{H}_{25})_{24}$ and $\text{Au}_{38}(\text{SC}_{12}\text{H}_{25})_{24}$ showing optical absorbance vs photon energy. The maximum energies of the first peaks are estimated to be 1.13 and 1.14 eV, respectively, for $\text{Au}_{38}(\text{SeC}_{12}\text{H}_{25})_{24}$ and $\text{Au}_{38}(\text{SC}_{12}\text{H}_{25})_{24}$.

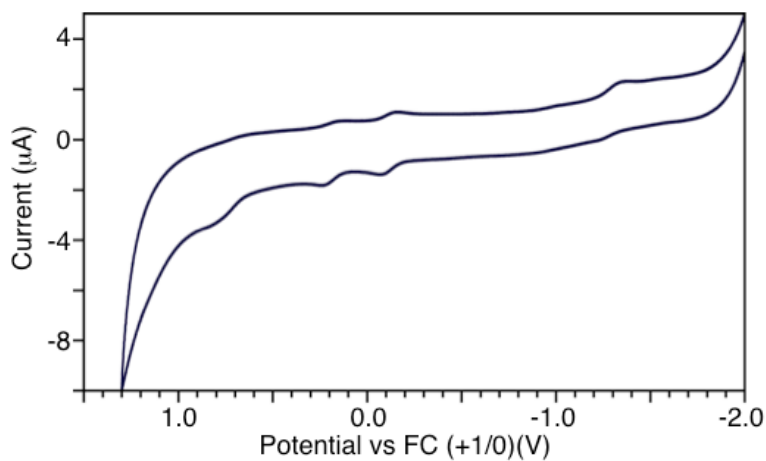


Figure S16. CV curve for $\text{Au}_{38}(\text{SeC}_{12}\text{H}_{25})_{24}$. These plots shows that $\text{Au}_{38}(\text{SeC}_{12}\text{H}_{25})_{24}$ is stable during redox reactions.

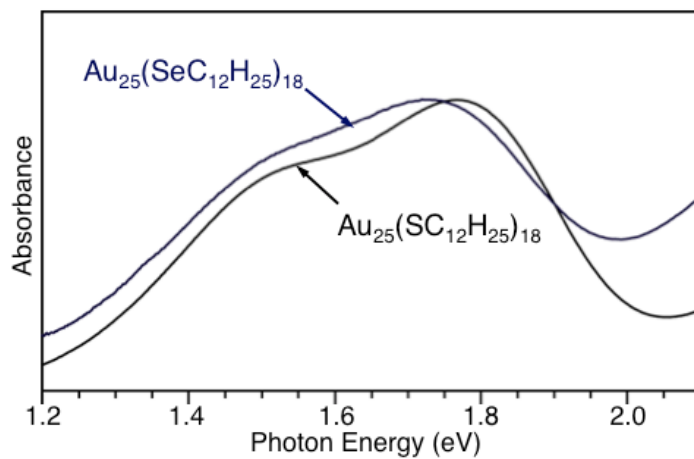


Figure S17. Enlarged optical absorption spectra of $\text{Au}_{25}(\text{SeC}_{12}\text{H}_{25})_{18}$ and $\text{Au}_{25}(\text{SC}_{12}\text{H}_{25})_{18}$ showing optical absorbance vs photon energy. The maximum energies of the first peaks are estimated to be 1.77 and 1.80 eV, respectively, for $\text{Au}_{25}(\text{SeC}_{12}\text{H}_{25})_{18}$ and $\text{Au}_{25}(\text{SC}_{12}\text{H}_{25})_{18}$.

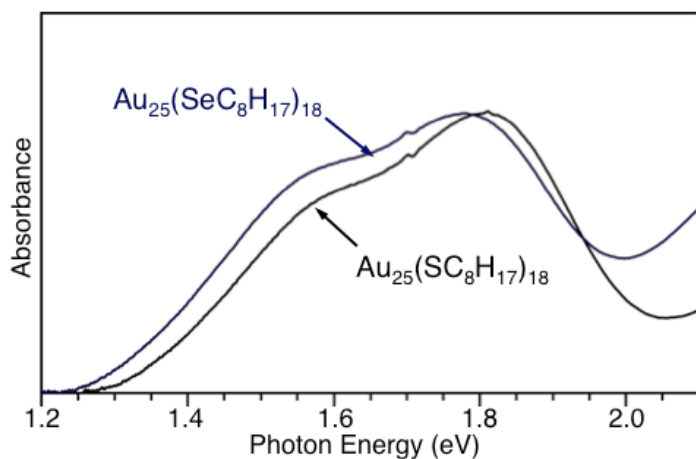


Figure S18. Enlarged optical absorption spectra of $\text{Au}_{25}(\text{SeC}_8\text{H}_{17})_{18}$ and $\text{Au}_{25}(\text{SC}_8\text{H}_{17})_{18}$ showing optical absorbance vs photon energy. The maximum energies of the first peaks are estimated to be 1.77 and 1.80 eV, respectively, for $\text{Au}_{25}(\text{SeC}_8\text{H}_{17})_{18}$ and $\text{Au}_{25}(\text{SC}_8\text{H}_{17})_{18}$.

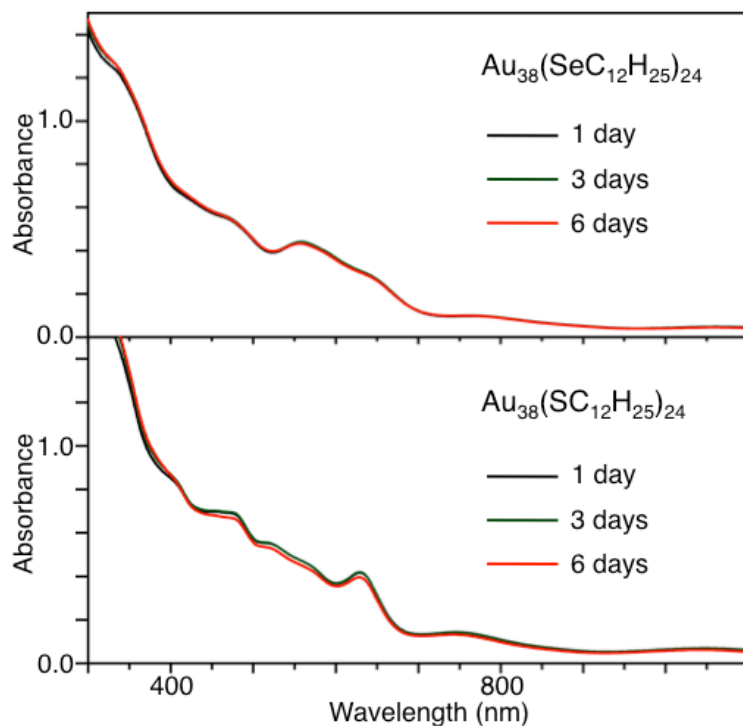


Figure S19. Variations over time in the absorption spectra of $\text{Au}_{38}(\text{SeC}_{12}\text{H}_{25})_{24}$ and $\text{Au}_{38}(\text{SC}_{12}\text{H}_{25})_{24}$ (both $1.0 \times 10^{-5} \text{ M}$) at 65°C .

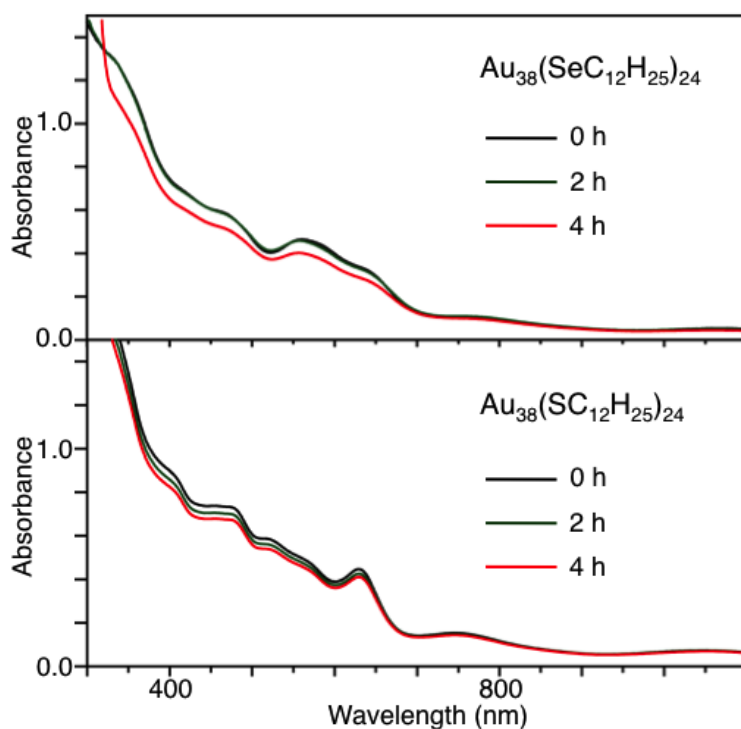


Figure S20. Variations over time in the absorption spectra of $\text{Au}_{38}(\text{SeC}_{12}\text{H}_{25})_{24}$ and $\text{Au}_{38}(\text{SC}_{12}\text{H}_{25})_{24}$ (both $1.0 \times 10^{-5} \text{ M}$) at 120°C . Both clusters degrade at the same rate, indicating that $\text{Au}_{38}(\text{SeC}_{12}\text{H}_{25})_{24}$ evidently has the same high level of stability as $\text{Au}_{38}(\text{SC}_{12}\text{H}_{25})_{24}$ in toluene. However, it has been reported that the stability of $\text{Au}_{38}(\text{SR})_{24}$ strongly depends on the solvent,²⁰ and the slight difference in stability between $\text{Au}_{38}(\text{SeC}_{12}\text{H}_{25})_{24}$ and $\text{Au}_{38}(\text{SC}_{12}\text{H}_{25})_{24}$ seen here could be amplified by changing the solvent.

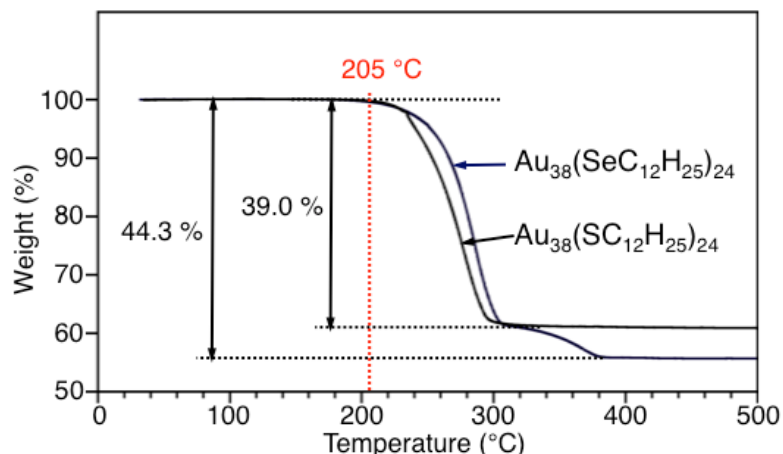


Figure S21. The relative resistances of solid $\text{Au}_{38}(\text{SeC}_{12}\text{H}_{25})_{24}$ and $\text{Au}_{38}(\text{SC}_{12}\text{H}_{25})_{24}$ to thermal dissociation. In these TG curves, the observed weight losses of 44.3 % and 39.0 % are consistent with the organic proportions in $\text{Au}_{38}(\text{SeC}_{12}\text{H}_{25})_{24}$ (44.3 %) and $\text{Au}_{38}(\text{SC}_{12}\text{H}_{25})_{24}$ (39.2 %), respectively. The temperature at which ligands begin to dissociate is estimated from the point at which the TGA curve starts to drop. As a result, barely any difference is seen between the two clusters, indicating that both clusters exhibit similar resistance to thermal dissociation in the solid state.

References

1. Negishi, Y.; Kurashige, W.; Kamimura, U. *Langmuir* **2011**, *27*, 12289.
2. Meng, X.; Xu, Q.; Wang, S.; Zhu, M. *Nanoscale* **2012**, *4*, 4161.
3. Qian, H.; Eckenhoff, W. T.; Zhu, Y.; Pintauer, T.; Jin, R. *J. Am. Chem. Soc.* **2010**, *132*, 8280.
4. Qian, H.; Zhu, M.; Andersen, U. N.; Jin, R. *J. Phys. Chem. A* **2009**, *113*, 4281.
5. Lopez-Acevedo, O.; Tsunoyama, H.; Tsukuda, T.; Häkkinen, H.; Aikens, C. M. *J. Am. Chem. Soc.* **2010**, *132*, 8210.
6. Qian, H.; Zhu, Y.; Jin, R. *ACS Nano* **2009**, *3*, 3795.
7. Brust, M.; Walker, M.; Bethell, D.; Schiffrin, D. J.; Whyman, R. *J. Chem. Soc., Chem. Commun.* **1994**, 801.
8. Negishi, Y.; Nobusada, K.; Tsukuda, T. *J. Am. Chem. Soc.* **2005**, *127*, 5261.
9. Negishi, Y.; Chaki, N. K.; Shichibu, Y.; Whetten, R. L.; Tsukuda, T. *J. Am. Chem. Soc.* **2007**, *129*, 11322.
10. Niihori, Y.; Kurashige, W.; Matsuzaki, M.; Negishi, Y. *Nanoscale* **2013**, *5*, 508.
11. Dass, A.; Stevenson, A.; Dubay, G. R.; Tracy, J. B.; Murray, R. W. *J. Am. Chem. Soc.* **2008**, *130*, 5940.
12. Ankudinov, A. L.; Ravel, B.; Rehr, J. J.; Conradson, S. D. *Phys. Rev. B* **1998**, *58*, 7565.
13. Negishi, Y.; Kurashige, W.; Kamimura, U. *Langmuir* **2011**, *27*, 12289.
14. Zeng, C.; Liu, C.; Pei, Y.; Jin, R. *ACS Nano* **2013**, *7*, 6138.
15. Qian, H.; Zhu, M.; Gayathri, C.; Gil, R. R.; Jin, R. *ACS Nano* **2011**, *5*, 8935.
16. Hasan, M.; Bethell, D.; Brust, M. *J. Am. Chem. Soc.* **2002**, *124*, 1132.
17. Xie, S.; Tsunoyama, H.; Kurashige, W.; Negishi, Y.; Tsukuda, T. *ACS Catal.* **2012**, *2*, 1519.
18. Kurashige, W.; Yamaguchi, M.; Nobusada, K.; Negishi, Y. *J. Phys. Chem. Lett.* **2012**, *3*, 2649.
19. MacDonald, M. A.; Chevrier, D. M.; Zhang, P.; Qian, H.; Jin, R. *J. Phys. Chem. C* **2011**, *115*, 15282.
20. Toikkanen, O.; Carlsson, S.; Dass, A.; Rönnholm, G.; Kalkkinen, N.; Quinn, B. M. *J. Phys. Chem. Lett.* **2010**, *1*, 32.